Spatially resolved Poisson strain and anticlastic curvature measurements in Si under large deflection bending

Wenge Yang, B. C. Larson,[a] G. E. Ice, J. Z. Tischler, J. D. Budai, and K.-S. Chung
Oak Ridge National Laboratory, Oak Ridge, Tennessee 37831

W. P. Lowe
Howard University, Washington, D.C. 20059

(Received 17 February 2003; accepted 3 April 2003)

A scanning-monochromatic form of differential-aperture x-ray microscopy (DAXM) has been developed that provides micron-resolution depth-resolved dilatational strain measurements. This scanning-monochromatic DAXM technique is applied to measurements of Poisson dilatational strain in 25-μm-thick Si bent into an arch with an apex radius of $R=3$ mm. Poisson strain measurements agree with anisotropic linear elasticity calculations for a Searle parameter as large as $\beta=1009$. Local anticlastic bend radii were shown to oscillate across the arch and reach the R/ν limit for distances less than the plate thickness from the edges, where ν is the anisotropic Poisson's ratio. © *2003 American Institute of Physics.* [DOI: 10.1063/1.1579857]

The energy balance between elastic bending and stretching strains is responsible for the rigidity of cylindrical plates and spherical shells and, accordingly, is central to a fundamental understanding of deformation such as in crumpling of sheets and membranes and the generation of singularities associated with axis normal deformation of cylinders and the formation of developed cones (i.e., coffee-filter like shapes).[1–4] Anticlastic curvature associated with lattice bending strains in elastically and plastically strained materials is technologically important for applications[5,6] ranging from springback in metal forming to the design of microelectromechanical systems.

Anticlastic bending in the small deflection regime has been investigated in detail.[7,8] However, high-resolution, spatially resolved diffraction techniques have not been available to investigate the interplay between anticlastic curvature and large deflection bending strains such as associated with crumpling and developed cone formation.[1–4]

Three-dimensional (3D) microbeam x-ray techniques for measuring grain-average elastic and plastic strain and grain-boundary mapping in polycrystals with $\sim 5-10$ μm spatial resolution or larger are available.[9] Moreover, submicron-resolution 3D crystal orientation and deviatoric (i.e., shear) strain measurements have been demonstrated using white beam differential-aperture x-ray microscopy (DAXM).[10,11] However, dilatation strain with micron depth resolution has not been available. In this letter we report the development of a scanning-monochromatic form of DAXM that makes it possible to perform micron-resolution, depth-resolved measurements of dilatational strain, and we apply this technique and microbeam Laue measurements to measure Poisson strain gradients and anticlastic curvature in strongly bent Si.[10] We emphasize that DAXM is a general technique for spatially resolving diffraction measurements; "scanning-monochromatic" DAXM measurements of the trace of the strain tensor (i.e., lattice dilatation) represent a specific adaptation of DAXM, as are the complementary "white-beam" DAXM measurements of the deviatoric component of the strain tensor reported earlier.[10] Both are required for the specification of full strain tensors in the general case.[11]

Figure 1 shows a schematic view of Si bent into the shape of an arch and the x-ray microbeam geometry on the MHATT–CAT and UNI–CAT beamlines at the Advanced Photon Source (APS).[10–12] These beamlines include undulator synchrotron x rays, removable/insertable scanning monochromators, Kirkpatrick–Baez focusing mirrors, charge coupled device (CCD) area x-ray detectors, and a Pt wire diffracted-beam profiler used in the DAXM measurements. In the present study, both white and monochromatic x-ray microbeams were focused to ~ 0.5 μm diameter.

Figure 1 also depicts the scattered beam for the scanning monochromatic DAXM method, which excites only one Bragg reflected beam. Measurements of surface-normal Poisson (dilatation) strains and strain gradients through the sample require scanning the energy of the monochromatic microbeam for each step of the (50 μm diameter Pt) profiler wire. This is in contrast to white beam DAXM, which is performed over $\sim 10-30$ Laue Bragg reflections.

Using the DAXM depth-profiling technique as described

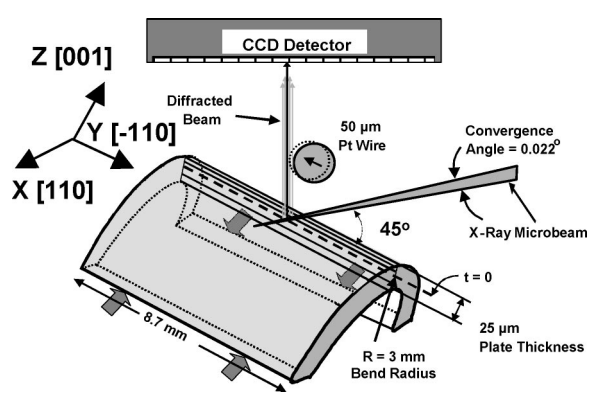

FIG. 1. Schematic of x-ray microbeam measurement geometry showing the wire profiler and the orientation of the cylindrically bent Si sample.

[a]Electronic mail: bcl@ornl.gov

previously,[10] pixel-by-pixel differences in the (008) Si Bragg peak intensities are calculated for CCD images collected before and after micron step of a 50 μm Pt wire and before and after each (1–2 eV) step of the monochromator energy. This makes it possible to determine both the scattering angle and the Bragg energy with micron depth resolution. As with white beam DAXM,[10] depth resolution is accomplished in DAXM by geometrical triangulation, where computer extrapolation of the optical path from individual CCD pixels to the Pt wire surface determines the scattering position at the microbeam.

Since the scanning-monochromatic form of DAXM requires depth profiling the Bragg energy and the Bragg angle of only one reflection, it is much less restrictive to apply than white-beam DAXM. This means that it can be performed using Fresnel zone plates or refractive x-ray lenses on monochromatic beam lines, avoiding the requirement of white beams and achromatic focusing optics.

The measurements here were performed on a 25 μm thick by 10.6 mm long by 8.74 mm wide rectangular Si plate oriented with a $\langle 001 \rangle$ surface normal and $\langle 110 \rangle$ edge normals. The plate was bent into the form of an arch (see Fig. 1) in which the principal bend radii were measured to be 2.95 ± 0.02 and 3.17 ± 0.02 mm at the two edges, and 3.06 ± 0.02 mm at the center, indicating a very slight cone shape to the arch, presumably as a result of mounting uncertainties. Although this bend is far into the large deflection regime, with a Searle parameter[8,13,14] of $\beta = (\text{width}^2)/(\text{radius} \cdot \text{thickness}) = 1009$, the brittle nature of Si at room temperature ensures that the strain is elastic.

The convergence angle of focused microbeams and strain gradients impact the energy width of Bragg reflections for depth-resolved diffraction measurements. For a cylindrically bent sample the energy width is given by $\Delta E/E = -[\text{ctg}(\theta)\Delta\theta + \Delta d/d]$, where E is the x-ray energy, θ is the Bragg angle, $\Delta\theta$ is the range of incident angles in the microbeam, and Δd is the range of d spacings within the spatially resolved diffraction volume (voxel). With $\Delta\theta$ taken to be the 0.022 degree convergence angle (see Fig. 1) of the microbeam, $\Delta d/d$ estimated to be $\sim 10^{-4}$ per micron for a bend radius of 3 mm, and including the 1.4 eV width of the 12 keV monochromatic beam, the energy width for a micron depth increment is ~ 5 eV. The energy of the Bragg reflection for each depth was obtained by performing a two-dimensional scan of x-ray microbeam energy versus the Pt wire profiler position (described earlier) and least-squares fitting to locate the centroid of the intensity distribution with ~ 0.5 eV precision for each depth.

For the anticlastic bending measurements, white-microbeam Laue diffraction was used to measure (depth-averaged) anticlastic rotations with a precision of better than 0.01 degrees for 20 μm steps along the 8.74 mm wide crest of the arch. The open circles in Fig. 2(a) indicate large, nearly 0.3° anticlastic rotations at the edges of the arch that oscillate in sign and decay to very small rotations in the middle of the arch. The curvature increases rapidly ~ 250 μm from the edge and reaches the limiting value of $(R/\nu)^{-1} = 0.021\ \text{mm}^{-1}$ for distances less than the (25 μm) plate thickness from the edges. Although the cylindrical curvature highly suppresses anticlastic bending in the central portion of the arch, a series of $\sim 0.01° - 0.02°$ oscillations/undulations appear to persist across the width of the arch. Figure 2(b) shows the local anticlastic curvatures, R_A^{-1} (radians/mm), as a function of position across the arch as determined from the slope of the local orientations in Fig. 2(a).

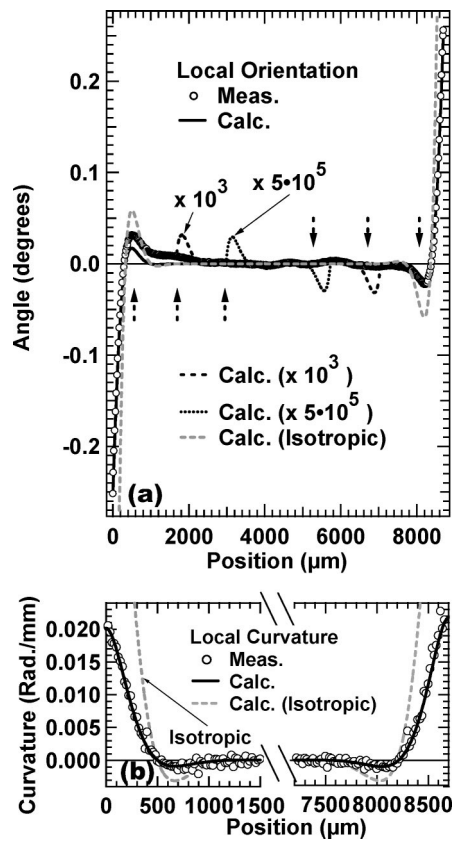

FIG. 2. The local anticlastic orientation (a) as a function of position along the crest of the arch measured by white microbeam diffraction (open circles) together with anisotropic (solid line) and isotropic (gray dashed line) elasticity calculations (solid line) and calculations scaled by 10^3 and 5×10^5 (dashed lines). The arrows are guides indicating the position of measured oscillations. Part (b) shows the measured (open circles) and calculated (solid line) local curvature determined from the derivative of the measured (open circles) and calculated (solid and dashed lines) orientations in part (a).

The solid line in Fig. 2(a) shows the theoretically predicted anticlastic bend orientations based on anisotropic, closed form solutions of the Föpl–Von Karman equations.[14–16] The anticlastic rotations predicted by the calculations are in good agreement with the rotations measured near the edges of the plate, including the position and magnitude of the oscillation that occurs at ≈ 500 μm from the edges. The gray (shaded) dashed lines in Figs. 2(a) and 2(b) show that much larger curvature would be present for isotropic (i.e., polycrystalline average, $\nu = 0.22$) Si than is observed for the [110] and [−110] in-plane directions of this sample, which has $\nu = 0.064$.[17] The small, but reproducible, oscillations that persist across the central portion of the arch have amplitudes that are more than 100 times larger than the exponentially damped amplitudes predicted by both linear elasticity[14,16] and finite element calculations.[18] The black dashed lines show segments of the calculations multiplied by 10^3 and 5×10^5, indicating that the positions and symmetry of the observed oscillations are correlated. Additional measurements and finite element calculations for varying bend

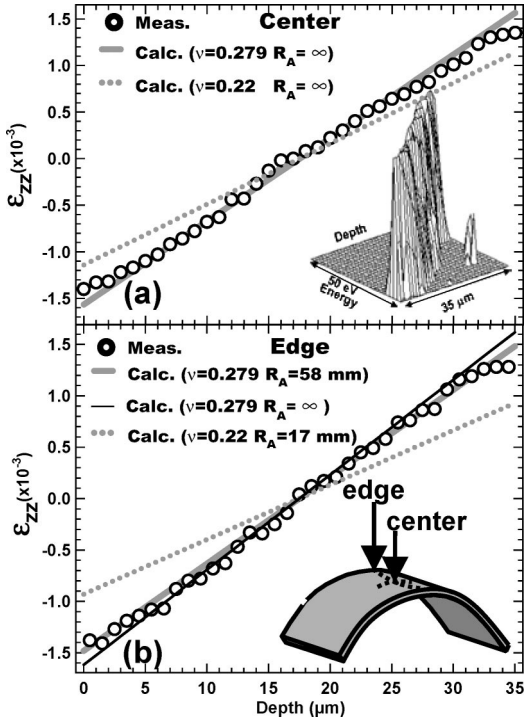

FIG. 3. Strain distributions as a function of depth at the center (a) and edge (b) positions of the cylindrically bent Si sample. The open circles are experimental measurements; the lines represent calculations in the thin plate approximation for the measured anticlastic radii of curvature (broad shaded line), no anticlastic affects (thin solid line), and isotropic average Poisson coupling (dotted line). The inset in (a) shows the Bragg diffraction intensity as a function of energy and depth for the strain measurement at the edge position.

conditions will be used to determine if the persistence of the oscillations is intrinsic or mounting induced.

Turning to the measurements of Poisson dilatational strain as a function of depth, Figs. 3(a) and 3(b) show micron-resolution depth-resolved strain measurements performed 100 μm from the edge of the arch and at the center of the arch. The inset in Fig. 3(a) shows scanning-monochromatic DAXM intensities measured for the Si (008) surface-normal reflection as a function of depth and energy. Least-squares fitting of a Gaussian function to the energy profile for each depth yielded the surface-normal Poisson strain, ε_{zz}, with micron depth resolution as plotted in Figs. 3(a) and 3(b) with $\pm 10^{-4}$ measurement uncertaintiess. In the thin-plate approximation, Landau and Lifshitz[19] show that

$$\varepsilon_{xx}=t/R; \qquad \varepsilon_{yy}=t/R_A; \qquad \varepsilon_{zz}=\frac{\nu}{\nu-1}\left(\frac{t}{R}+\frac{t}{R_A}\right), \qquad (1)$$

where t is the distance in the thickness direction from the midplane of the plate (see Fig. 1). The strain calculated using Eq. (1) (including the measured primary and anticlastic radii of curvature) is plotted as the broad shaded lines in Figs. 3(a) and 3(b). In contrast to the very small $\nu=0.064$ for the [110] and [−110] in-plane direction, the Poisson's ratio for the [001] and [110] out of plane direction is 0.279. The dilatation measurements (open circles) are in agreement with the predicted values both at the center and the edge of the arch, within the estimated $\pm 10^{-4}$ measurement uncertainties. The gray dotted lines in Figs. 3(a) and 3(b) illustrate the Poisson coupling strain expected for polycrystalline isotropic Si.

It is important to note that the scanning-monochromatic DAXM technique measures the dilatational strain directly, whereas previous depth resolved[10] measurements using white beam DAXM required independent knowledge that anticlastic bending was negligible at the center of the arch (i.e., $\varepsilon_{yy}\approx 0$). This distinction is of critical importance for fundamental strain investigations.

We have introduced a scanning monochromatic form of DAXM that provides dilatational strain measurements with micron depth resolution, and we have used this technique in combination with white beam Laue measurements to study anticlastic curvature and Poisson dilatational strain in the very large deflection regime ($\beta=1009$) for Si.

The authors thank I. C. Noyan for discussions and L. B. Freund for making finite element calculations, and they acknowledge the help of E. M. Dufresne, W. Liu, and E. Williams during this project. This research was sponsored by the US Department of Energy, Basic Energy Sciences, Division of Materials Sciences under Contract No DE-AC05-00OR22725 with Oak Ridge National Laboratory, managed by UT-Battelle, LLC; work performed on the MHATT–CAT beamline at the APS was supported in part by DOE Grant No. DE-FG02-99ER45743; UNI–CAT is operated by UIUC, ORNL, NIST, and UOP Research, Inc. The operation of the APS is sponsored by the DOE.

[1] A. E. Lobkovsky, Phys. Rev. E **53**, 3750 (1996).
[2] A. Boudaoud, P. Patricio, Y. Couder, and M. Ben Amar, Nature (London) **407**, 718 (2000).
[3] S. Chaïeb, F. Melo, and J.-C. Géminard, Phys. Rev. Lett. **80**, 2354 (1998).
[4] A. Lobkovsky, S. Gentges, H. Li, D. Morse, and T. A. Witten, Science (Washington, DC, U.S.) **270**, 1482 (1995).
[5] W. D. Carden, L. M. Geng, D. K. Matlok, and R. H. Wagoner, Int. J. Mech. Sci. **44**, 79 (2002).
[6] A. C. M. Chong, F. Yang, D. C. C. Lam, and P. Tong, J. Mater. Res. **16**, 1052 (2001).
[7] J. P. Quintana, V. I. Kushnir, and G. Rosenbaum, Nucl. Instrum. Methods Phys. Res. A **362**, 592 (1995).
[8] S. K. Kaldor and I. C. Noyan, Appl. Phys. Lett. **80**, 2284 (2002).
[9] H. F. Poulsen, S. F. Nielsen, E. M. Lauridsen, S. Schmidt, R. M. Suter, U. Lienert, L. Margulies, T. Lorentzen, and D. Juul Jensen, J. Appl. Crystallogr. **34**, 751 (2001).
[10] B. C. Larson, W. Yang, G. E. Ice, J. D. Budai, and J. Z. Tischler, Nature (London) **415**, 887 (2002).
[11] J.-S. Chung and G. E. Ice, J. Appl. Phys. **86**, 5249 (1999).
[12] G. E. Ice and B. C. Larson, Adv. Eng. Mater. **2**, 643 (2000).
[13] I. C. Noyan and J. B. Cohen, *Residual Stress: Measurement by Diffraction and Interpretation* (Springer, New York, 1987).
[14] D. G. Ashwell, J. R. Aeronaut. Soc. **54**, 708 (1950).
[15] Y. C. Pao, J. Compos. Mater. **4**, 380 (1970).
[16] S. R. Swanson, Compos. Struct. **53**, 449 (2001).
[17] W. A. Brantley, J. Appl. Phys. **44**, 534 (1973).
[18] L. B. Freund (private communication).
[19] L. D. Landau and E. M. Lifshitz, *Theory of Elasticity*, 3rd ed. (Pergamon, New York, 1986).